ARTICLE

Ternary Copper (II) complexes of 1,10-phenanthroline and coumarin-based oxylacetates as pro-apoptotic UPR CHOP inducer

Received 00th January 20xx,
Accepted 00th January 20xx

DOI: 10.1039/x0xx00000x

Sebastiano Masuri[a], Maria Grazia Cabiddu[a], Lukáš Moráň[b,b], Tereza Vesselá[b], Martin Bartosik[c], Josef Havel[d,e], Francesca Meloni[a], Enzo Cadoni[a], Petr Vaňhara[b,d], Tiziana Pivetta[*,a]

We prepared six complexes with formula $[Cu(phen)_2(L_x)](ClO_4)$(x: 1 – 6) where the auxiliary ligands L_x are coumarin carboxylate derivatives bearing an oxylacetate moiety in the 6th or 7th position and different substituents in the 3rd or 4th position. Complexes show a pentacoordinated geometry around the metal ion. The possibility to complete the coordination sphere in an octahedral geometry makes the molecule able to further react. Complexes show affinity toward DNA mainly through electrostatic interactions and groove binding, while the interactions with dna base pairs are guaranteed by the auxiliary ligands. The heteroleptic Cu(II) complexes show cytotoxic activity in the micromolar concentration range, and mechanistic studies have pointed out how they can interfere at Endotelial Reticulum level inducing the pro-apoptotic branch of the Unfoled Protein Response (UPR). The actin-normalized chop to bip density ratios suggest that the novel compounds induce preferentially the pro-apoptotic UPR signalling driven by chop, in a dose-dependent way and according to the substituents in the coumarinic moiety.

Introduction

The accidental discovery in 1960s of the antiproliferative activity of cisplatin (cis-diaminodichloroplatin (II)) has provided a new perspective in terms of application of coordination compounds in medicine.[1] Despite that cisplatin and its derivatives are currently used in the treatment of several types of cancers, their efficacy is affected by several dose-dependent side effects, along with a high incidence of acquired or inherited resistance.[2–5] In the design of new potential metal-based drugs that overcome the limitations just cited, substitution of Pt(II) with endogenous metal ions has been commonly exploited. The rationale behind this approach is that complexes of essential metal ions may show lower systemic toxicity and take advantage of the molecular machinery involved in transport and homeostasis of endogenous metal ions.[6] Moreover, these complexes may interact with DNA differently than Pt(II)-based drugs, or trigger cell death by targeting different molecular pathways and/or biomolecules.[7] Copper is a typical example of endogenous ion, that shares with cisplatin the same transporter protein hCtr1.[8] Many nitrogen-containing ligands, such as 1,10-phenantroline have been tested for their antitumor activity on different human cancer cell lines, both alone and as part of metal complexes. In the former case, an increase in potency compared to the ligand alone is commonly observed, probably related to an enhanced ability of the molecule to cross biological barrier and/or to act with different action mechanisms. Additional modulation in terms of biological properties might also be achieved through the insertion of auxiliary ligands in the metal coordination sphere.[9–12] We had prepared several mixed Cu(II)-phenanthroline complexes bearing different auxiliary ligands, finding that these compounds show potent cytotoxic properties in several human cancer cells.[13,14] Recent studies have pointed out that these complexes induce in ovarian (A-2780 and SKOV-3) cancer cells pro-apoptotic branch of Unfolded Protein Response (UPR), which is activated in condition of prolonged or severe Endoplasmic Reticulum (ER) stress.[15,16]

All these remarks have prompted us to further investigate on the cytotoxicity of ternary Cu(II)-phenanthroline complexes with auxiliary ligands. We considered coumarin-based oxylacetates since coumarins show high versatility in terms of pharmacological properties, such as antimicrobial, anti-inflammatory, antioxidant and anticancer ones.[17–20] For example, the naturally occurring coumarins 2-H-cromen-2-one and umbelliferone (7-hydroxy-2-H-cromen-2-one), have shown potent cytotoxic and cytostatic activity,[21] and mixed complexes containing a dioxylacetate derivative of aesculetin (6,7-dihyroxy-2-H-cromen-2-one) have shown high potency in terms of antiproliferative activity.[22]

In this study, we prepared six complexes with formula $[Cu(phen)_2(L1)](ClO_4)$(x: 1 – 6) where the auxiliary ligands (L1-6,

[a.] *Department of Chemical and Geological Sciences, University of Cagliari, Cittadella Universitaria, 09042, Monserrato, Cagliari, Italy. E-mail tpivetta@unica.it*
[b.] *Department of Histology and Embryology, Faculty of Medicine, Masaryk University, 62500, Brno, Czech Republic.*
[c.] *Research Centre for Applied Molecular Oncology, Masaryk Memorial Cancer Institute, 65653 Brno, Czech Republic*
[d.] *International Clinical Research Center, St. Anne's University Hospital, 65691, Brno, Czech Republic.*
[e.] *Department of Chemistry, Faculty of Science, Masaryk University, 62500, Brno, Czech Republic.*
Electronic Supplementary Information (ESI) available: [details of any supplementary information available should be included here]. See DOI: 10.1039/x0xx00000x

Figure 1) are coumarin carboxylate derivatives bearing an oxylacetate moiety in the 6th or 7th position and different substituents in the 3rd or 4th position. The obtained copper complexes (D1-D6, Fig. 1) were studied in both solid and solution state by means of different experimental and computational techniques. D1-D6 were tested *in-vitro* on ovarian (SKOV-3) cancer cells. Mechanistic studies on the most promising compounds of the series have pointed out how they can interfere at ER level inducing the pro-apoptotic branch of the UPR. Moreover, considering that DNA constitutes a potential target of several anticancer compounds, we evaluated the DNA affinity and the potential mechanism of interaction by combining the experimental measurements with theoretical calculations.

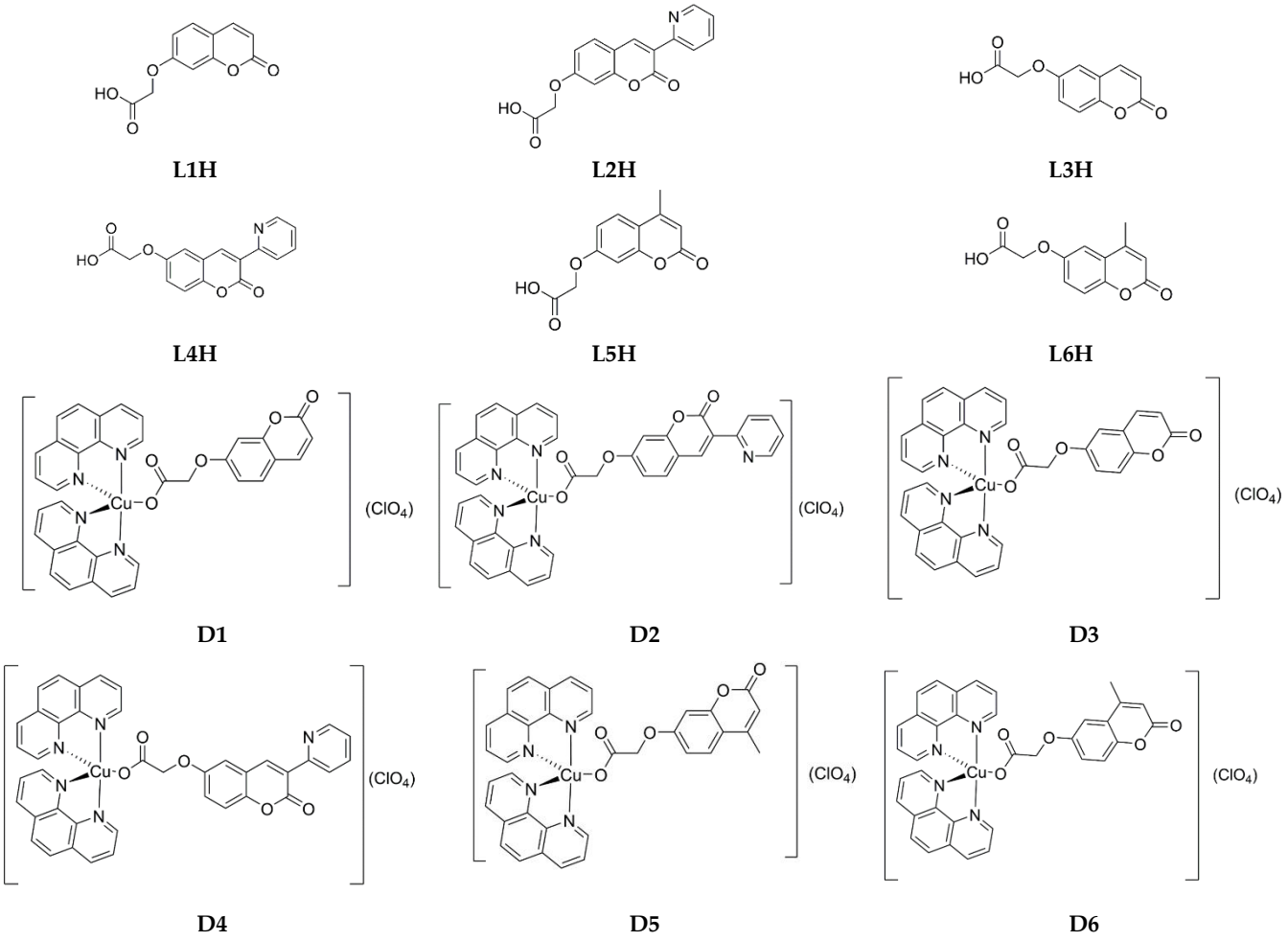

Fig. 1. Structure and acronyms of the studied ligands (**L^{x}H**) and Cu(II) complexes (**D1-D6**).

Results and discussion

Synthesis of ligands

The ligands LxH (x = 1 – 6) were obtained from hydroxylated derivatives 1a-f through nucleophilic substitution with ethyl bromoacetate using K_2CO_3 as base. The former ethyl esters 2a-f were submitted to basic hydrolysis followed by acidification to obtain the carboxylic acids LxH. The synthetic pathway is reported in Scheme 1.

Synthesis of copper(II) complexes

The novel mixed coumarin-phenanthroline Cu(II) complexes with general formula $[Cu(phen)_2(Lx)](ClO_4)$ (D1-D6, where x = 1 - 6) have been obtained by reacting the obtained in-situ sodium salts of HL1-6 with the precursor $[Cu(phen)_2(OH_2)](ClO_4)_2$ (C0). The stoichiometries of D1-D6 have been assessed through UV-Vis (see "Complexes stoichiometries and formation constants" section) and ESI-MS measurements. In all the ESI-MS spectra, the most intense peak was due to the $[Cu(phen)_2(Lx)]^+$ species (Fig. S1-6), obtained from the corresponding D1-D6 complex by loss of the perchlorate anion. The identification of the reported ions was confirmed by the fitting of the experimental isotopic patterns (Fig. S7) and by Tandem Mass experiments (see "Tandem MS" section).

Both ligands and Cu(II) complexes are stable in the solid state at room temperature. They are soluble in DMSO up to 0.1 M concentration level, in CH_3CN at 0.02 M, and in the H_2O:CH_3CN mixture (1:1) at 0.01 M. Solubility in water is achieved by dissolving the studied compounds in DMSO (e.g. 2.0 mM) prior

to dilution with distilled water or aqueous buffer (they are soluble at 20 µM concentration in 99:1 aqueous buffer:DMSO). In this case, sonication or vigorous mixing should be avoided to prevent the formation of emulsions. Stock solutions in DMSO and CH_3CN are stable at 4 °C up to 6 months, while stock solutions in H_2O:CH_3CN mixture (1:1) could be stored at r.t. for 2 weeks. The stability of the complexes in aqueous medium was evaluated by preparing 6.0 µM solutions in phosphate buffer (0.05 M pH 7.4) and following the spectral variation in the 200–450 nm range for 24 hrs by recording 1 spectrum every 60 minutes. No significant variations in the shape and intensity of the spectra were observed for any of the studied complexes. The UV-Vis spectra of D2, recorded under this experimental setup, are reported as an example in the Supporting (Fig. S8).

Scheme 1. Reagents and conditions: a) K_2CO_3, ethyl bromoacetate, acetone rf 24 hrs; b) 5% NaOH (aq), methanol, rf 24 hrs, HCl 2.0 N till pH acid.

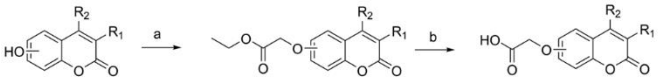

1a: $R_1 = R_2$ = -H ; -OH 7th position
1b: R_1 = pyridin-2-yl ; R_2 = -H; -OH 7th position
1c: $R_1 = R_2$ = -H ; -OH 6th position
1d: R_1 = pyridin-2-yl; R_2 = -H; -OH 6th position
1e: R_1 = -CH_3 ; R_2 = -H; -OH 7th position
1f: R_1 = -CH_3 ; R_2 = -H; -OH 6th position

2a: $R_1 = R_2$ = -H ; -$OCH_2CO_2C_2H_5$ 7th position
2b: R_1 = pyridin-2-yl ; R_2 = -H; -$OCH_2CO_2C_2H_5$ 7th position
2c: $R_1 = R_2$ = -H ; -$OCH_2CO_2C_2H_5$ 6th position
2d: R_1 = pyridin-2-yl; R_2 = -H; -$OCH_2CO_2C_2H_5$ 6th position
2e: R_1 = -CH_3 ; R_2 = -H; -$OCH_2CO_2C_2H_5$ 7th position
2f: R_1 = -CH_3 ; R_2 = -H; -$OCH_2CO_2C_2H_5$ 6th position

Complex coordination mode

Since no suitable crystals for X-Ray structure determination were afforded for any of the studied complexes, the coordination around the metal ion was confirmed by combining different experimental and theoretical results.

UV-Vis. Molecular absorption spectra of D1-D6 in the region 400 - 1100 nm are reported in Fig. S9. All the spectra feature a maximum at approx. 700 nm and a shoulder at approx. 950 nm. In accordance with the absorption spectra of ternary Cu(II) bis-phenanthroline complexes previously characterized, [13] a penta-coordinated geometry might be proposed also for the novel complexes reported in this study.

FT-IR. The coordination mode of the ligand carboxylate group around the metal centre was investigated by FT-IR spectroscopy. As commonly known, carboxylate groups can coordinate metal ions as unidentate, chelating or bridging ligand. The parameter $\Delta(OCO)=\nu_{asym}(OCO)-\nu_{sym}(OCO)$ is used to determine the coordination mode adopted by carboxylates upon complexation: unidentate mode when $\Delta(OCO)_{complex}>\Delta(OCO)_{ligand}$, chelating when $\Delta(OCO)_{complex}<\Delta(OCO)_{ligand}$, bridging when $\Delta(OCO)_{complex}\approx\Delta(OCO)_{ligand}$.[23,24] By the analysis of the IR spectra, the carboxylic group appears to coordinate the metal centre in a monodentate fashion in all the complexes. The IR spectra of D1, L1 and C0 are reported as an example in Fig. S10.

Mass spectrometry (+). Mass spectra were recorded to confirm the hypothesised complexes, and Collision Induced Dissociation (CID) mass experiments were carried out at different collision energies (CE, 0-50 V) to have more information about the structure of the synthesized complexes. As reported before, in all the complexes the most intense peak was due to the species $[Cu(phen)_2(Lx)]^+$, for loss of a perchlorate anion from the neutral molecule $Cu(phen)_2(Lx)(ClO_4)$. The coordination mode of the ligands was determined by the CID experiments, in particular from the analysis of the metal containing fragments. The CID experiments of the D1's parent ion at 642 *m/z* ($[Cu(phen)_2(L1)]^+$) is reported and explained in the Supporting as an example (Fig. S11). The same fragmentation patterns were observed for all the studied complexes. In some cases a peak at *m/z* 243 due to the species $[Cu(phen)]^+$ is obtained for the loss of the L1 moiety as radical, with subsequent reduction of Cu(II) centre. The reduction of Cu(II) to Cu(I) is often observed in ESI phase, depending on the solvent. [16,25]

Theoretical calculations. Geometry optimizations for ligands and complexes were performed by the computational setup used for C0, whose coordinates were taken from its crystal structure, as previously discussed.[16] Geometry optimization of L^1 was achieved starting from the X-Ray crystal structure of dimethylammonium 2-[(2-oxo-2H-chromen-7-yl)oxy]acetate [26], showing a good agreement between experimental and calculated structural parameters (Table S1). Structures of the DFT-optimized geometries of L1-6 are shown in Fig. S12, while selected bond lengths, angles and dihedrals calculated for $L2^-$L6 are reported in Tables S2–S6. Molecular electrostatic potential (MEP) surfaces are reported in Fig. S13 and S14 for ligands and complexes. As expected, the highest electron density is localised on the carboxylate anions, with trend: L5 (-708 kj) < L4 (-707 kj) < L6 (-706 kj) < L3 (-704 kj) < L2 (-699 kj) < L1 (-646 kj). The lowest electron density zones vary in the order L1 (-82 kj) < L5 (-35 kj) < L6 (-33 kj) < L3 (-19 kj) < L2 (6 kj) < L4 (17 kj).

As regards the metal complexes, the highest electron density is localised on the auxiliary ligands, in particular on the coumarinic carbonylic oxygen, with trend: D6 (-168 kj) < D5 (-166 kj) < D3 (-159 kj) < D1 (-154 kj) < D4 (-140 kj) < D2(-132 kj). The most positive zones are, instead, localised on the phenanthroline moieties, with similar entity for all the molecules, ranging from +406 to +414 kj (D6 > D5 = D3 > D1 > D4 > D2).

From the analysis of the ligand frontier molecular orbitals (Fig. S15, Table S9) it is possible to observe that HOMOs are mainly centred on the carboxylate moiety, supporting the hypothesis that these compounds can coordinate the metal ion using this functional group. This assumption finds further confirmation by the high negative atomic charges on the carboxylate oxygens (see Tables S7-8). Geometry optimization of D1-D6 complexes (Fig. 3) suggest a pentacoordinate geometry, closer to a square pyramidal than a trigonal bipyramidal, as indicated by the values of "tau" geometrical parameter ($\tau=(\beta-\alpha)/(60°)$) reported in Table S16. The adoption of such geometry is also evident at bond length level. In fact, taking the structural parameters of $[Cu(phen)_2(L1)]^+$ (Table S10) as example, it is possible to observe that the elongation of Cu-N2 (2.285 Å) is accompanied by the shortening of Cu-N1, Cu-N3, Cu-N4 and Cu-O1 bonds (2.045,

2.030, 2.087 and 1.986 Å respectively). These results are in agreement with the experimental metrics of several mono and binuclear Cu(II) bis-phenanthroline complexes, coordinated by carboxylate functional groups.[27–30] Selected bonds, angles, and dihedrals for the other copper complexes are reported in Tables S11-S15.

The analysis of the atomic charges calculated at natural population analysis (NPA) level (Tables S17-18) shows on the copper ion a significant lower atomic charge (1.39) compared with its formal charge +2, while on N1-4 and O1 atoms high negative calculated charges are evidenced. This trend might be indicative of a Ligand to Metal Charge Transfer (LMCT), as observed by comparing β-SOMOs, mainly centred on the coumarin-based moiety, and β-LUMOs, distributed among the metal centre and one of the phenanthroline molecules (Fig. S16-18). Energies (in eV) of complexes frontier orbitals are reported in Table S19.

Complexes formation study

The complexes formation between C0 and the deprotonated ligands L1-6 was studied in water solution by the method of continuous variations (Job's method). At the chosen experimental conditions, the studied ligands exist as monoanionic species due to the loss of the carboxylic proton. For all the ligands, formation of only one complex with metal:ligand 1:1 molar ratio (χ_L=0.5) was proved. No binuclear complexes were observed with deprotonated L2 and L4, where the nitrogen 3-pyridinyl and coumarin carbonyl could represent a potential chelating site.[31,32] In Fig. S19A spectra collected varying the ligand molar ratio from 0 to 10 for the system C0 - L2 are reported as an example. Absorbance data at 344, 292 and 270 nm, corrected for the absorption contribution of the reactants, clearly indicate the formation of a 1:1 molar ratio complex (Fig. S19B). The formation of the mononuclear complex was further assessed by spectrophotometric titration: by adding the ligands, a decrease in intensity of C0 band at 270 nm and the formation of a new band in the range 320-340 nm was observed, together with an isosbestic point at approx. 300 nm, indicating the presence of at least one equilibrium in solution. From eigenvalue analysis of the spectrophotometrical data in the 225–400 nm range, three significant eigenvalues were found, indicative of three linearly independent absorbing species, i.e. $[Cu(phen)_2]^{2+}$, $[Cu(phen)_2L]^{+}$, and $[L]^{-}_{free,exc}$. The formation constants were calculated for all the complexes (Table 1). Selected spectra recorded during the titrations are reported in Fig. 4.

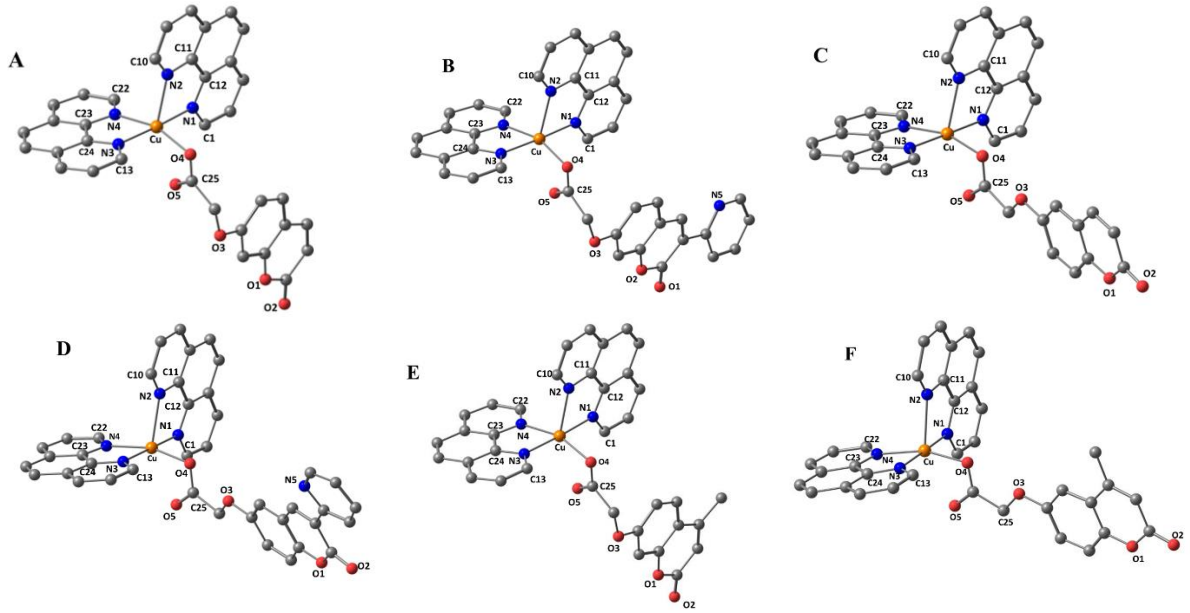

Fig. 3. Molecular drawings and atom labelling scheme for $[Cu(phen)_2(L1)]+$ (A), $[Cu(phen)_2(L2)]+$ (B), $[Cu(phen)_2(L3)]+$ (C), $[Cu(phen)_2(L4)]+$ (D), $[Cu(phen)_2(L5)]+$ (E), $[Cu(phen)_2(L6)]+$ (F) at the DFT-optimized geometries (gas phase).

Biological Evaluation

ct-DNA interaction studies. The affinity of the synthesised compounds towards ct-DNA was studied by UV-Vis Spectroscopy. Selected spectra of deprotonated ligands and copper complexes in presence of increasing amounts of ct-DNA are reported in Fig. S20 and Fig. S21, respectively. A general increase in absorbance was observed in the 240-285 nm range in the presence of DNA. In some cases (e.g., L1 and D2) a decrease in absorbance, from moderate to low, in the 305-400 nm region was observed, together with the appearance of an isosbestic point in the 295-303 nm range. From the eigenvalue analysis of the spectrophotometric data in the 250-400 nm region three significant eigenvalues were found, indicative of three linearly independent absorbing species, i.e. the free DNA, the free ligand or complex, and the DNA adduct. By fitting the experimental data considering a 1:1 adduct, the related binding constants were calculated (Table 2).

Table 1. Complex formation constants and calculated spectral properties for the studied complexes (25 °C, PB 0.05 M, pH 7.4). The standard deviation to the last significant figure is reported in parentheses.

Species	Logβ	Absorption maxima (nm)	Calculated absorptivity (10^4 $M^{-1}cm^{-1}$)
$[Cu(phen)_2(L1)]^+$	5.03(2)	272, 321 (sh)	5.11, 1.72
$[Cu(phen)_2(L2)]^+$	5.1(1)	272, 344	5.23, 2.44
$[Cu(phen)_2(L3)]^+$	4.3(1)	272, 321 (sh)	5.70, 0.75
$[Cu(phen)_2(L4)]^+$	4.7(1)	272, 344	5.82, 0.60
$[Cu(phen)_2(L5)]^+$	5.85(7)	271, 318 (sh)	5.65, 1.36
$[Cu(phen)_2(L6)]^+$	6.0 (1)	272, 322 (sh)	6.36, 0.61

The DNA binding constants are in the order: L5 > L6 > L3 ≈ L4 > L2 > L1 for the ligands, and in the order D5 > D3 > D4 > D2 > D6 > D1 for the copper complexes. Complexes show generally more affinity toward DNA than ligands alone. As commonly known, changes in the spectra profile are indicative of the interaction mode with DNA.[33] Absorption spectra of small intercalating molecules generally show hypochromism (> 35%) and bathochromic shift (> 15 nm).[34] Compounds that act as groove binders and/or interact through electrostatic interaction generally cause hyperchromism. The collected spectrophotometrical data indicate that these compounds target ct-DNA mainly through electrostatic interactions and groove binding. This is further confirmed from the analysis of the pure spectra of the absorbing species, calculated from the eigenvalue analysis (Fig. S22-23).

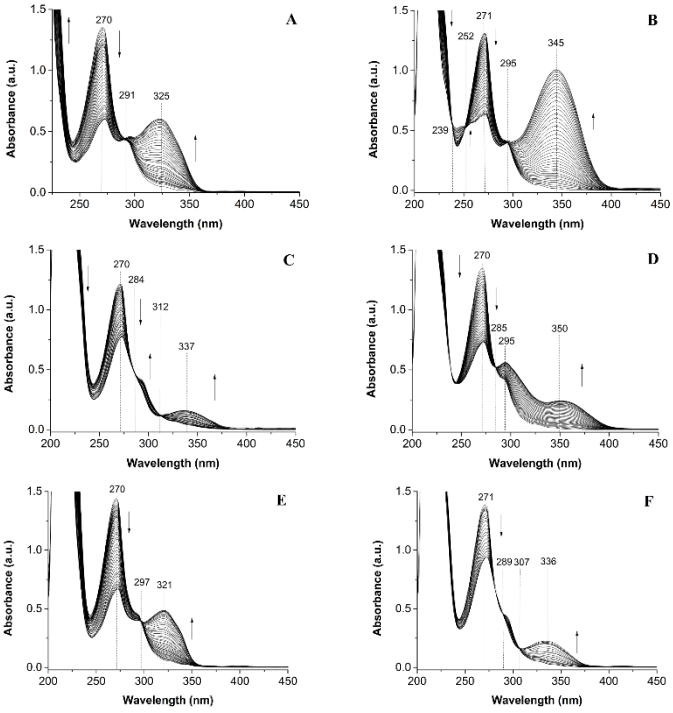

Fig. 4. Selected spectra collected during the spectrophotometric titration of C0 with (A) L1 (C0 5.368·10-5mmoles, L1 6.177·10-5 M), (B) L2 (C0 5.304·10-5mmoles, L2 6.325·10-5 M), (C) L3 (C0 4.680·10-5mmoles, L3 5.450·10-5 M), (D) L4 (C0 5.462·10-5mmoles, L4 5.046·10-5 M), (E) L5 (C0 5.368·10-5mmoles, L5 6.490·10-5M), (F) L6 (C0 5.304·10-5mmoles, L4 6.405·10-5M) ; PB 0.05 M, pH 7.4, 25 °C, 1 cm optical path length.

Table 2. DNA-binding constants for the studied compounds and % hypochromism (at λmax, for R = [DNA]/[compound] = 4) for selected ones (25 °C, TRIS-HCl buffer, pH 7.1). The standard deviation to the last significant figure is reported in parentheses.

Molecule	K_b (M^{-1})x10^4	% Hypochromism*	λ_{max} nm
L1	3.8(3)	13.2	324
L2	6.4(3)	14.1	344
L3	12(5)	-	
L4	13(5)	11.9	354
L5	400(8)	10.7	319
L6	130(6)	-	
D1	5.6(4)	8.4	324
D2	32(7)	9.7	364
D3	100(4)	-	
D4	79(8)	2.0	355
D5	200(5)	3.7	322
D6	7.9(4)	-	
C0	10(5)	-	

*Calculated as $(A_f-A_b/A_f)\cdot100$, A_f and A_b are the absorbance in absence and presence of ct-DNA respectively

The possibility of a partial intercalative mode for those compounds that showed some hypochromic effect in the 305-400 nm (L1, L2, L4, L5, D1, D2, D4) can be ruled out since the % of hypochromism, calculated at λmax, considering an excess of ct-DNA (R = [DNA]/[compound] = 4) appears to be quite low (from 2 to 14 %, Table 2).

Molecular docking. Docking simulations were performed to better clarify the binding mechanism between the deprotonated ligands L1-6, C0, $[Cu(phen)_2(Lx)]^+$ and B-DNA. Ligands interact at the minor groove of the DNA double helix (Fig. S24), in agreement with the experimental results obtained from UV-Vis spectroscopy. Compounds L1, L2 and L5 possess a similar not-covalent interactions profile, forming a hydrogen bond with G10 base using their lactonic oxygen atoms (Fig. S25). A different hydrogen bonding profile is observed for L4 and L6 with respect to L3, where the oxylacetic group is in the 6th position: the introduction of substituents in the coumarinic structure (a pyridyl ring in L4, a methyl in L6) induces a 180° twist in the conformation orientation (compared to L3), determining a different hydrogen bonding profile (Fig. S26).
As regards the complexes, all of them are positioned in proximity of one of the minor grooves (Fig. 5), in agreement with the experimental findings from UV-Vis. As expected, the bulky $[Cu(phen)_2]^{2+}$ moiety is in proximity of the phosphate backbone, thus supporting the possibility of establishing electrostatic interactions, while the interactions with DNA base pairs are guaranteed by the auxiliary ligands for the coumarin-based molecules for $[Cu(phen)_2(Lx)]^+$ species. The hydrogen bonding profile for the studied complexes are shown in Fig. S27.

Cytotoxicity. The cytotoxicity of the studied compounds was evaluated in-vitro on ovarian (SKOV-3) cancer cells. Results, expressed as IC_{50} values, i.e. concentration of drug able to induce cell death in 50% of cells, are summarized in Table 3 and shown in Figure 6. As observed, the heteroleptic Cu(II) complexes D1-D6 shows cytotoxic activity in the micromolar concentration range, while the corresponding coumarin-based oxylacetatic acids are devoid of activity in the concentration range explored. Moreover, D1-D5 complexes show IC50 lower than the precursor C0. These results confirm the importance of the metal complex structure in exerting the anticancer potency and are not attributable only to the Cu2+ ion, as previously demonstrated 15. Although there are not such big differences in terms of IC_{50} values, compounds D2 and D5 (differently substituted in the 3rd and 4th positions, both bearing an oxylacetate in the 7th position) seem to be the most promising of the series, showing a cytotoxicity four times higher than C0. Viability % of the D1-D6 compounds (from MTT data) at different treatments were reported in Fig. S28.

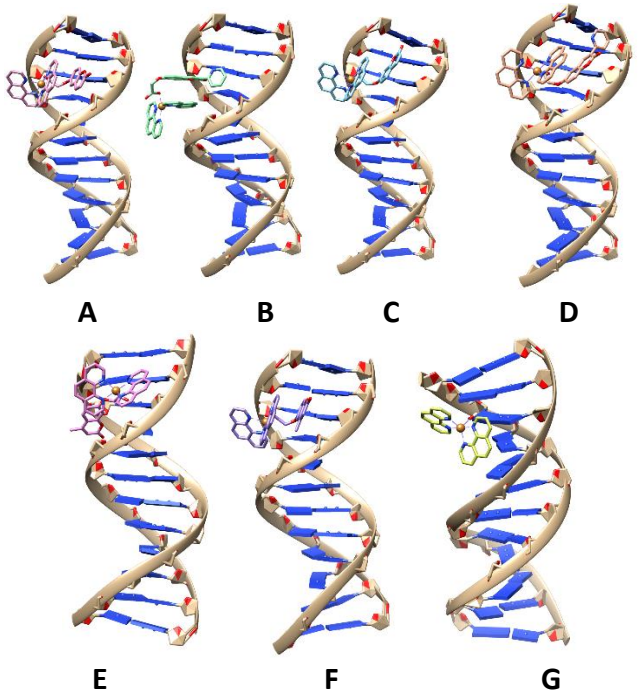

Fig. 5. Full view of the complex between the highest-ranking score of $[Cu(phen)_2(Lx)]^+$ (x = 1 – 6) and BDNA (A-F). Full view of the complex between the highest-ranking score of $[Cu(phen)_2(OH_2)]^{2+}$ and BDNA (G).

Mechanistic studies. When cells experience the ER stress, a high concentration of misfolded proteins is accumulated in the endoplasmic reticulum. In cells that are under ER stress, the misfolded proteins bind to the ER-chaperone Binding Immunoglobulin Protein (BiP, GRP-78), which in turn leaves three proteins, the Protein kinase R (PKR)-like Endoplasmic Reticulum Kinase (PERK), the Inositol-Requiring Enzyme 1 (IRE1) and the Activating Transcription Factor 6 (ATF6), that initiate three distinct branches of UPR. A more detailed description of the downstream pathways activated by these proteins is reported elsewhere.[35,36]

Table 3. Cytotoxicity of the studied compounds reported as IC50 values from MTT data after 24 hrs treatment. Results were obtained from technical hexaplicates in 3 independent experiments.

Compound	IC_{50} ± SD (μM)
D1	3.0 ± 0.6
D2	2.1 ± 0.1
D3	2.6 ± 0.2
D4	5 ± 2
D5	2.0 ± 0.7
D6	3.4 ± 0.3
L1-6	> 10
C0	7.9 ± 0.1

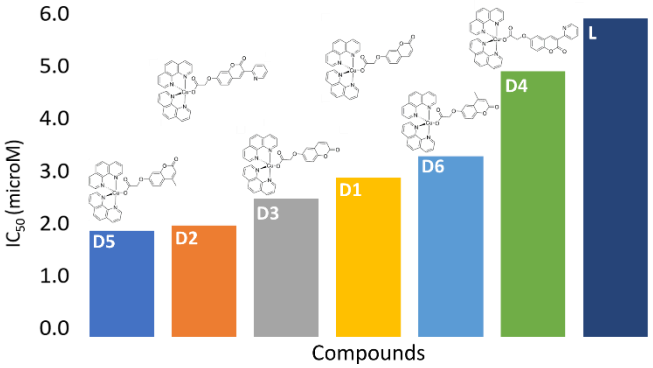

Fig. 6. The cytotoxic in-vitro effects of the studied compounds evaluated on ovarian (SKOV-3) cancer cells expressed as IC50 values (concentration of drug able to induce cell death in 50% of cells) and the structural formula of the studied compounds.

During this initial phase, the UPR tries to alleviate the ER workload to allow the elimination of the misfolded proteins and restore the normal functioning of this cellular organelle. However, when the ER stress is prolonged and/or severe, the UPR can arrest cell-cycle progression and ultimately induce the apoptosis. Under these circumstances, the expression of the pro-apoptotic signaller C/EBP homologous protein (CHOP) is up-regulated, as observed upon cell treatment with the ER stress inducer Tunicamycin, which inhibits the N-glycosylation of proteins.[37] Considering the ability of similar mixed Cu(II) bis-phenanthroline complexes in inducing the pro-apoptotic branch of the UPR,[12,15,16] we monitored the expression of BiP and CHOP in the most promising compounds of the series, D2 and D5, also including D1 and C0 for structural comparisons. In previous study we had observed in SKOV-3 cells that in the presence of C0, the chaperone BiP (HSPA5) and the pro-apoptotic protein CHOP (DDIT3) were both upregulation in a 5:1 ratio, and also the transcription factor ATF6 level appeared increased [submitted manuscript]. As regard the test on D1, D2 and D5, the Actin-normalized CHOP to BiP density ratios, derived from Western Blot results (Fig. 7), suggest that these novel compounds induce preferentially the pro-apoptotic UPR signalling driven by CHOP when compared to the ctrl and C0. Interestingly, the entity of these variations is dose-dependent and structurally related, according to the substituents in the

coumarinic moiety. In fact, the presence of a methyl group in the 4th position of the coumarinic backbone, as in D5, significantly up-regulates the CHOP expression level even at sub-lethal concentrations (1.0 μM). These findings confirm the ability of these ternary Cu(II) complexes to induce cell death by activating the pro-apoptotic branch of UPR. The exact molecular mechanism how these complexes act within the ER needs, however, to be clarified.

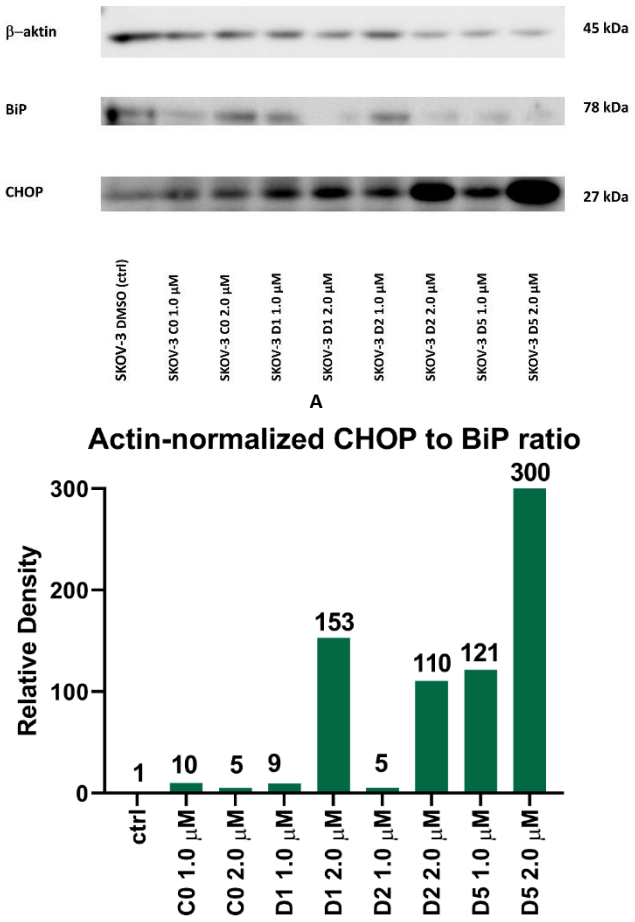

Fig. 7. (A) Protein expression of BiP and CHOP in SKOV-3 cells treated for 24 hrs with C0, D1, D2 and D5 at sub-lethal (1.0 μM) and lethal concentrations (2.0 μM). β-Actin was used as a control of equal loading. (B) Actin-normalized CHOP to BiP density ratios, calculated from immunoblotting results on SKOV-3 cells

QSAR Evaluation

In an attempt to find a correlation between structure and activity for compounds D1-D5, we performed the Principal Component Analysis on the following experimental and calculated parameters: MEP min and max values (min, max), the accessible area of the molecule (acc.area), the octanol/water partition coefficient (P), the dipole moment (dipole), the DNA binding constant (DNA), the complex stability constant (beta), and the cytotoxic activity (IC_{50}). At first, we considered both ligands and complexes, finding a clear separation between the two classes of compounds (Fig. 8). Ligands (red ellipse) were characterized by the higher IC_{50} values, with respect to the copper complexes (green ellipse). The principal component PC1 resulted to be directly dependent mainly on the electron density map values and indirectly on IC_{50}, while the second component PC2 was dependent on the DNA binding constant.

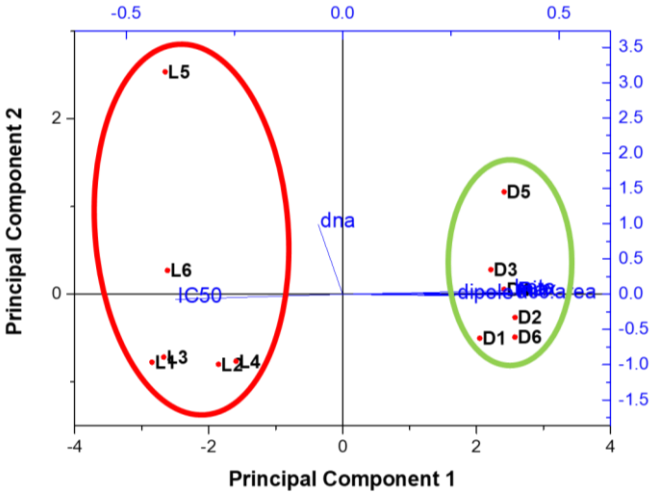

Fig. 8. Principal Component Analysis for ligands and complexes. Biplot of scores (ligands and complexes) and loadings (variables). PC1 = 0.393 min + 0.397max + 0.395acc.area + 0.398P -0.057DNA -0.389IC_{50} + 0.391beta + 0.260dipole; PC2 = 0.021min + 0.026max - 0.012acc.area + 0.001P + 0.995DNA - 0.071IC_{50} + 0.051beta - 0.021dipole (min is the minimum value of the MEP, max is the maximum value of the MEP, acc.area is the accessible area of the molecule, P is the octanol/water partition coefficient, dipole is the dipole moment, DNA is the DNA binding constant, beta is the complex stability constant, IC_{50} is for the cytotoxic activity).

The variables related to the electron density (min, max, P, acc.area) appear directly correlated with the complex formation constant and indirectly correlated with the IC_{50}, while the DNA binding constant does not appear correlated with any other variables.

Considering only the copper complexes (Fig. 9) and selecting the five most important variables (to perform PCA the number of the variables should be lower than that of the object), it is possible to observe that D1, D2 and D3 are located nearby, differently from D4, D5 and D6. D4 is characterised by a high IC_{50} values, being in effect the less toxic compound, while D5 is characterised by a low IC_{50} value and a high stability constant and results to be the more toxic complex. D1, D2, D3 and D6, being close to the PC1 axis, are not described by the PC1 loadings but only by PC2 loadings, in particular by the dipole moments and the stability constant. IC_{50} and dipole moments appear to be directly correlated, while DNA binding constants appear also in this case uncorrelated with the other variables.

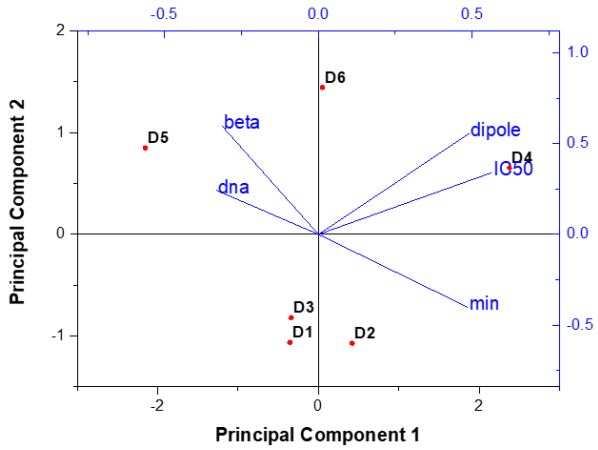

Fig. 9. Principal Component Analysis for complexes. PC1 = 0.484min - 0.331DNA + 0.564IC_{50} - 0.314beta + 0.489dipole, PC2 = -0.400min + 0.242DNA + 0.340IC_{50} + 0.600beta + 0.554dipole (min is the minimum value of the MEP, dipole is the dipole moment, DNA is the DNA binding constant, beta is the complex stability constant, IC_{50} is for the cytotoxic activity).

Conclusions

A panel of novel heteroleptic Cu(II)-phenanthroline complexes with oxylacetic acids substituted coumarins were prepared. The novel compounds show interesting biological properties. They are able to interact with DNA, mainly through electrostatic interactions and groove binding, and induce cell death on ovarian (SKOV-3) cancer cells, provoking the activation of the pro-apoptotic branch of the UPR. Differently from their precursor C0, the signaller CHOP is strongly upregulated, in a dose-dependent way and in dependence of kind and position of the substituents.

The chemometric analysis of the experimental and theoretical data show that the antiproliferative effect is poorly related to the interaction with DNA, confirming that the biological action can be exerted on multiple targets[38] and also with different kinetic.

The cross-disciplinarity (chemistry, biochemistry, molecular biology, medicine) of this study and the results achieved therein could be useful in the design and synthesis of novel potential anticancer metal-based drugs that could target alternative pathways with respect that currently approved Pt(II)-based chemotherapeutics.

Experimental

Materials and methods

Reagents. Acetonitrile, methanol, ethanol, isopropanol, acetone, DNA, tris (hydroxymethyl)aminomethane hydrochloride (TRIS-HCl), sodium chloride, deuterated chloroform, sodium hydroxide, dimethyl sulfoxide and hydrochloric acid were purchased from Merck (Milan, Italy). MTT reagent (3-(4,5-dimethylthiazol-2-yl)-2,5-diphenyltetrazolium bromide) and Tween-20 were purchased from Merck (Czech Republic). Potassium carbonate, copper(II) carbonate hydroxide, ethyl bromoacetate, deuterated dimethyl sulfoxide, 7-hydroxycoumarin, 6-hydroxycoumarin, 7-hydroxy-4-methylcoumarin, 6-hydroxy-4-methylcoumarin 2,4-dihydroxybenzaldehyde, 2,5-dihydroxybenzaldehyde and pyridine 2-acetonitrile were purchased from Alfa-Aesar. The commercial reagents were used as received, without any further purification. Ultrapure water was obtained with a MilliQ Millipore apparatus.

NMR. ^{1}H and ^{13}C NMR spectra were recorded on Varian 500 and Bruker Advance III HD 600 spectrometers at room temperature with tetramethylsilane (TMS) as internal standard in DMSO d6 or $CDCl_3$. Chemical shifts, multiplicity and coupling constants were reported.

FT-IR. Infrared spectra were recorded with a Bruker Vector 22 spectrophotometer, preparing the samples as KBr pellets.

Solution equilibria. UV–Visible spectrophotometric measurements were performed on an Agilent Cary 60 spectrophotometer in the range 200–500 nm using a 1 cm quartz cell at 25 °C. The formation constants of the complexes formed by C0 with the studied ligands were determined by spectrophotometric titration in phosphate buffer (PB) 0.05 M solution. Complex stoichiometries were also evaluated by means of the Job's method.[39,40]

The intrinsic binding constants (Kb) between ct-DNA and the studied compounds were determined at 25 °C by spectrophotometric titrations in TRIS-HCl buffer (TRIS-HCl 0.05 M, NaCl 0.05 M) at pH 7.1. Stock solutions of ct-DNA were prepared in TRIS-HCl buffer at pH 7.1 and stored at 4.0 °C within 96 hrs. The concentration of DNA per nucleotide was checked by UV absorption at 260 nm using its molar absorption coefficient (6600 M−1 cm−1). DNA purity was verified by determining the A280nm/A260nm ratio: a value ≥ 1.8 is indicative of a sufficiently protein-free DNA.[41,42] Solutions having a fixed amount of ligand/metal complex (9.78 10^{-6} M to 1.24 10^{-5} M according to compounds solubility and absorptivity) were titrated at 25 °C by adding increasing volumes of ct-DNA (2.27 10^{-4} M) and recording the UV-Vis spectrum. The number of linearly independent absorbing species was obtained by applying eigenvalues analysis on the absorbance data matrix. The complex formation constants (expressed as overall association constants) were calculated using the Hyperquad 2006 program.[43]

Mass spectrometry. Mass spectra were recorded using a triple quadrupole QqQ Varian 310-MS mass spectrometer using the atmospheric pressure ESI technique. The sample solutions were infused directly into the ESI source using a programmable syringe pump at a flow rate of 1.25 mL/h. A dwell time of 14 s was used, and the spectra were accumulated for 5 min to increase the signal-to-noise ratio. Mass spectra were recorded in the *m/z* 100–1000 range. Optimised parameters for metal ion complex analysis were adopted.[44] The isotopic patterns of the

measured peaks in the mass spectra were analysed using the mMass 5.5.0 software package.[45,46]

Theoretical calculations. DFT calculations were performed using the release 4.2.0 of the ORCA software package.[47] Input files for DFT calculations were prepared using Avogadro 1.2.0.[48] Geometry optimizations were performed using the hybrid PBE0 functional [49] 51 and def-2 TZVP basis set,[50] as previously reported for similar systems 16. [16] The nature of the minima in each optimization was evaluated by assessing the absence of negative frequencies in the calculated IR spectra. Atomic charges at natural population analysis (NPA) level were calculated by means of JANPA software package 53. [51] Molecular orbital shapes and energies were investigated using Chemcraft v1.8 54. [52]

Molecular docking calculations were performed using the Autodock Vina software 55. [53] The X-Ray structure of BNA (PDB: 1BNA) was chosen as receptor. Both ligands and receptor were prepared using MG Labs Autodock Tools before docking 56. [54] In the receptor, water molecules were removed while polar hydrogens and Gasteiger charges were added. For all the ligands, non-polar hydrogens were removed, Gasteiger charges were added while no rotational constraints were applied. In the complexes, the atomic charges for copper were manually adjusted in the generated pdbqt files. All the tested compounds were docked using a grid cube of 30 × 30 × 42 points, centred at coordinates x = 14.780, y = 20.976, z = 8.807, with a spacing of 1.0 Å and an exhaustiveness value of 100. Molecular interactions and docked poses were evaluated using USCF Chimera 1.15 57. [55]

Synthesis of ligands. *Synthesis of hydroxy-3-(pyridin-2-yl)coumarin derivatives **1b** and **1d**.* Both compounds were prepared as previously reported [32,56]. *Synthesis of coumarin oxyacetic ethylic esters derivatives **2a-f**:* K_2CO_3 (5.83 mmol, 1.5 eq.) was added in one portion at r.t. to a suspension of hydroxylated coumarin **1a-f** (3.89 mmol) in acetone (20 mL). The mixture was stirred for approx. 15 minutes, then ethyl bromoacetate (0.65 mL, 5.83 mmol, 1.0 eq.) was added. The reaction mixture was kept under reflux for 24 hours. The resulting solution was filtered and the solvent was evaporated under reduced pressure, affording a solid that was recrystallized from ethanol.

Ethyl 2-((2-oxo-2*H*-chromen-7-yl)oxy)acetate (2a). White solid. Yield was 67%. Spectral data are consistent with those reported in literature [57]. ^{1}H-NMR (600 MHz, $CDCl_3$, δ, ppm, Fig. S29): 7.64 (d, J = 9.5 Hz, 1H), 7.40 (d, J = 8.6 Hz, 1H), 6.90 (dd, J = 8.6, 2.5 Hz, 1H), 6.78 (d, J = 2.5 Hz, 1H), 6.28 (d, J = 9.5 Hz, 1H), 4.68 (s, 2H), 4.29 (q, J = 7.1 Hz, 2H), 1.32 (td, J = 7.1, 0.8 Hz, 3H). ESI-MS, *m/z*, found (calcd) 249.0 (249.1) $[M+H]^+$.

Ethyl 2-((2-oxo-3-(pyridin-2-yl)-2*H*-chromen-7-yl)oxy)acetate (2b). White solid. Yield was 44%. ^{1}H-NMR (500 MHz, DMSO d_6, δ, ppm, Fig. S30): 8.86 (s, 1H), 8.69 (ddd, J = 4.8, 1.9, 1.0 Hz, 1H), 8.27 (dt, J = 8.1, 1.1 Hz, 1H), 7.93 – 7.85 (m, 2H), 7.41 (ddd, J = 7.5, 4.7, 1.2 Hz, 1H), 7.08 (d, J = 2.5 Hz, 1H), 7.04 (dd, J = 8.6, 2.5 Hz, 1H), 4.97 (s, 2H), 4.21 (q, J = 7.1 Hz, 2H), 1.24 (t, J = 7.1 Hz, 3H). ESI-MS, *m/z*, found (calcd): 326.2 (326.1) $[M+H]^+$.

Ethyl 2-((2-oxo-2*H*-chromen-6-yl)oxy)acetate (2c). Beige solid. Yield was 67%. Spectral data are consistent with those reported in literature.[58] ^{1}H-NMR (600 MHz, $CDCl_3$, δ, ppm, Fig. S31): 7.64 (d, J = 9.5 Hz, 1H), 7.28 (d, J = 9.0 Hz, 1H), 7.15 (dd, J = 9.0, 3.0 Hz, 1H), 6.94 (d, J = 3.0 Hz, 1H), 6.44 (d, J = 9.5 Hz, 1H), 4.66 (s, 2H), 4.29 (q, J = 7.1 Hz, 2H), 1.31 (t, J = 7.2 Hz, 3H). ESI-MS, *m/z*, found (calcd) 249.1 (249.1) $[M+H]^+$.

Ethyl 2-((2-oxo-3-(pyridin-2-yl)-2*H*-chromen-6-yl)oxy)acetate (2d). Beige solid. Yield was 45%. ^{1}H-NMR (600 MHz, $CDCl_3$, δ, ppm, Fig. S32): 8.71 (s, 1H), 8.68 (ddd, J = 4.7, 1.9, 1.0 Hz, 1H), 8.43 (dt, J = 8.1, 1.1 Hz, 1H), 7.82 – 7.77 (m, 1H), 7.34 (d, J = 9.0 Hz, 1H), 7.31 (ddt, J = 6.8, 4.8, 1.0 Hz, 1H), 7.20 (ddd, J = 9.0, 2.9, 0.8 Hz, 1H), 7.06 (d, J = 3.0 Hz, 1H), 4.67 (s, 2H), 4.32 – 4.27 (m, 2H), 1.32 (td, J = 7.1, 0.8 Hz, 3H). ESI-MS, *m/z*, (calcd): 326.2 (326.1) $[M+H]^+$.

Ethyl 2-((4-methyl-2-oxo-2*H*-chromen-7-yl)oxy)acetate (2e). White solid. Yield was 84%. Spectral data are consistent with those reported in literature. [59] ^{1}H-NMR (600 MHz, $CDCl_3$, δ, ppm, Fig. S33): 7.53 (d, J = 8.8 Hz, 1H), 6.92 (dd, J = 8.8, 2.6 Hz, 1H), 6.78 (d, J = 2.6 Hz, 1H), 6.16 (q, J = 1.3 Hz, 1H), 4.68 (s, 2H), 4.29 (q, J = 7.1 Hz, 2H), 2.40 (d, J = 1.2 Hz, 3H), 1.32 (t, J = 7.1 Hz, 3H). ESI-MS, *m/z*, found (calcd): 262.2 (262.1) $[M+H]^+$.

Ethyl 2-((4-methyl-2-oxo-2*H*-chromen-6-yl)oxy)acetate (2f). White solid. Yield was 88%. Spectral data are consistent with those reported in literature.[59] ^{1}H-NMR (600 MHz, $CDCl_3$, δ, ppm, Fig. S34): 7.29 (d, J = 8.9 Hz, 1H), 7.12 (dd, J = 8.9, 3.0 Hz, 1H), 7.10 (d, J = 2.9 Hz, 1H), 6.31 (d, J = 1.5 Hz, 1H), 4.67 (s, 2H), 4.29 (q, J = 7.2 Hz, 2H), 2.41 (d, J = 1.3 Hz, 3H), 1.31 (t, J = 7.1 Hz, 3H). ESI-MS, *m/z*, found (calcd): 262.1 (262.1) $[M+H]^+$.

*Synthesis of coumarin oxyacetic acid derivatives (**HL^1-^{6}**).*

Compound **2a-f** (1.60 mmol) was dissolved in 7.0 mL of ethanol. 4.0 mL (3 eq.) of NaOH 5% solution were added in one portion at r.t. and the reaction mixture was kept under reflux for 24 hours. The solution was concentrated under reduced pressure to ~ half the volume, then 6.0 mL of distilled water were poured and HCl 2.0 N were added drop by drop until acidic pH was reached. A solid compound precipitated slowly from the solution. It was filtered under vacuum and recrystallized from ethanol.

2-((2-oxo-2*H*-chromen-7-yl)oxy)acetic acid (**HL^1**)**.** White solid. Yield was 58%. Spectral data are consistent with those reported in literature[60]. ^{1}H-NMR (600 MHz, DMSO d_6, δ, ppm, Fig. S35): 1H NMR (600 MHz, DMSO-d6) δ 13.09 (s, 1H), 8.00 (d, J = 9.5 Hz, 1H), 7.65 (dd, J = 9.0, 2.0 Hz, 1H), 6.97 – 6.95 (m, 2H), 6.31 (d, J = 9.4 Hz, 1H), 4.82 (s, 2H). ESI-MS, *m/z*, found (calcd) 218.5 (219.0) $[M-H]^-$, 438.5 (439.0) $[2M-H]^-$.

2-((2-oxo-3-(pyridin-2-yl)-2*H*-chromen-7-yl)oxy)acetic acid (HL^2). Light yellow solid**.** Yield was 48%. ^{1}H-NMR (600 MHz, DMSO d_6, δ, ppm, Fig. S36) 12.98 (s, 1H), 8.76 (s, 1H), 8.63 (ddd, J = 4.7, 1.8, 0.9 Hz, 1H), 8.21 (dd, J = 8.1, 1.1 Hz, 1H), 7.84 (td, J = 7.8, 1.9 Hz, 1H), 7.44 (d, J = 3.0 Hz, 1H), 7.38 – 7.36 (m, 1H), 7.35 (d, J = 9.0 Hz, 1H), 7.21 (dd, J = 9.0, 3.0 Hz, 1H), 4.69 (s, 2H). ^{13}C-NMR (151 MHz, DMSO d6, δ, ppm, Fig. S37): 170.35, 160.01, 154.72, 151.45, 149.94, 148.52, 142.72, 137.24, 125.45, 124.17, 123.98, 120.81, 120.04, 117.41,

113.01, 65.42. ESI-MS, *m/z*, found (calcd): 298.0 (298.1) $[M+H]^+$, 320.2 (320.1) $[M+Na]^+$.

2-((2-oxo-2*H*-chromen-6-yl)oxy)acetic acid (HL^3). Light pink solid. Yield was 65%. Spectral data are consistent with those reported in literature[58]. ^{1}H-NMR (600 MHz, DMSO d_6, δ, ppm, Fig. S38): ^{1}H-NMR (600 MHz, DMSO d_6, δ, ppm): 13.15 (s, 1H), 8.01 (d, J = 9.6 Hz, 1H), 7.35 (d, J = 9.0 Hz, 1H), 7.27 (d, J = 3.0 Hz, 1H), 7.22 (dd, J = 9.0, 3.0 Hz, 1H), 6.49 (d, J = 9.6 Hz, 1H), 4.73 (s, 2H). ESI-MS, *m/z*, found (calcd) 218.5 (219.0) $[M-H]^-$, 438.5 (439.0) $[2M-H]^-$.

2-((2-oxo-3-(pyridin-2-yl)-2*H*-chromen-6-yl)oxy)acetic acid (HL^4). Brown solid. Yield was 42%. ^{1}H-NMR (600 MHz, DMSO d_6, δ, ppm, Fig. S39): 8.89 (s, 1H), 8.73 (ddd, J = 4.8, 1.9, 0.9 Hz, 1H), 8.30 (dt, J = 8.1, 1.1 Hz, 1H), 7.93 (td, J = 7.8, 1.9 Hz, 1H), 7.90 (d, J = 8.5 Hz, 1H), 7.44 (ddd, J = 7.5, 4.7, 1.1 Hz, 1H), 7.09 – 7.03 (m, 2H), 4.88 (s, 2H).^{13}C-NMR (151 MHz, DMSO d_6, δ, ppm, Fig. S40): 170.05, 162.12, 160.14, 155.61, 151.68, 149.81, 143.04, 137.18, 131.08, 123.69, 123.52, 121.61, 113.62, 113.58, 101.39, 65.64. ESI-MS, *m/z*, found (calcd) 298.3 (298.1) $[M+H]^+$, 320.0 (320.1) $[M+Na]^+$, 335.9 (336.0) $[M+K]^+$.

2-((4-methyl-2-oxo-2*H*-chromen-7-yl)oxy)acetic acid (HL^5). White solid. Yield was 72%. Spectral data are consistent with those reported in literature [59]. ^{1}H-NMR (600 MHz, DMSO d^6, δ, ppm, Fig. S41): 13.22 (s, 1H), 7.75 (d, J = 8.7 Hz, 1H), 7.04 (dd, J = 8.7, 2.6 Hz, 1H), 7.02 (d, J = 2.5 Hz, 1H), 6.29 (q, J = 1.3 Hz, 1H), 4.88 (s, 2H), 2.46 (d, J = 1.2 Hz, 3H). ESI-MS, *m/z*, found (calcd) 232.9 (233.0) $[M-H]^-$, 467.2 (467.1) $[2M-H]^-$.

2-((4-methyl-2-oxo-2*H*-chromen-6-yl)oxy)acetic acid (HL^6). Brown solid. Yield was 62%. Spectral data are consistent with those reported in literature [59]. ^{1}H-NMR (600 MHz, DMSO d_6, δ, ppm, Fig. S42): 13.09 (s, 1H), 7.37 – 7.33 (m, 1H), 7.24 (dt, J = 4.5, 2.4 Hz, 2H), 6.41 (d, J = 1.4 Hz, 1H), 4.79 (s, 2H), 2.42 (d, J = 1.3 Hz, 3H). ESI-MS, *m/z*, found (calcd) 233.0 (233.0) $[M-H]^-$, 467.0 (467.1) $[2M-H]^-$.

*Synthesis of sodium 2-((2-oxo-2H-chromen-7-yl)oxy)acetate (**NaL^1**).* Compound **HL^1** (0.104 mmol) was suspended in 3.0 mL of acetonitrile, then 104 µL of NaOH 1.0 M solution (0.104 mmol, 1.0 eq) were added to the reaction mixture, that was left under stirring at r.t. for 5 hrs. A light brown solid was isolated by filtration, which was washed repeatedly with acetonitrile and dried under vacuum. Yield was 56 %. Elemental analysis, exp (calc.): C 55.19% (54.16%), H 2.98% (2.91%). FT-IR (KBr), cm^{-1}: 1696 ($\upsilon(CO)_{ester}$), 1615 ($\upsilon(OCO)_{asym}$), 1416 ($\upsilon(OCO)_{sym}$).

Synthesis of copper complexes. $[Cu(phen)_2(OH_2)](ClO_4)_2$ (C0) was prepared as previously described [15,61]. $[Cu(phen)_2(L1)](ClO_4)$ (D1) was prepared as follows: HL1 (0.46 mmol) was treated with 4.6 mL of NaOH 0.1 M solution (0.46 mmol, 1.0 eq.) to obtain the corresponding sodium salt. The former solution was added to a suspension of C0 (0.46 mmol, 1.0 eq.) in 4.6 mL of methanol. The progressive formation of a pale blue precipitate was observed. Reaction mixture was left under stirring at room temperature for 24 hours. The desired product was recovered by filtration under vacuum, washed with water, ethyl ether and air dried. 0.2740 g (81%). Elemental analysis, exp (calc.): C 55.85% (56.61%), H 3.03% (3.12%), N 7.47% (7.55%). ESI-MS, *m/z*, found (calc.): 641.2 (641.1) $[Cu(phen)_2(L^1)]^+$ (Fig. S1). FT-IR (KBr), cm^{-1}: 1728 ($\upsilon(CO)_{ester}$), 1611 ($\upsilon(OCO)_{asym}$), 1362 ($\upsilon(OCO)_{sym}$).

$[Cu(phen)_2(L^2)](ClO_4)$ (D2) was prepared as described above, starting from 0.22 mmol of HL2. The product was obtained as a light green powder 0.1427 g (70%). Elemental analysis, exp (calc.): C 58.35% (58.61%), H 3.11% (3.20%), N 8.46% (8.54%). ESI-MS, *m/z*, found (calc.): 719.1 (719.1) $[Cu(phen)_2(L2)]^+$ (Fig**.** S2). FT-IR (KBr), cm^{-1}: 1716 ($\upsilon(CO)_{ester}$), 1608 ($\upsilon(OCO)_{asym}$), 1402 ($\upsilon(OCO)_{sym}$).

$[Cu(phen)_2(L^3)](ClO_4)$ (D3) was prepared as described above, starting from 0.39 mmol of HL3. The product was obtained as a light green powder 0.2700 g (93%). Elemental analysis, exp (calc.): C 56.40% (56.61%), H 2.98% (3.12%), N 7.40% (7.55%). ESI-MS, *m/z*, found (calc.): 641.2 (641.1) $[Cu(phen)_2(L3)]^+$ (Fig. S3). FT-IR (KBr), cm^{-1}: 1720 ($\upsilon(CO)_{ester}$), 1612 ($\upsilon(OCO)_{asym}$), 1366 ($\upsilon(OCO)_{sym}$).

$[Cu(phen)_2(L^4)](ClO_4)$ (D4) was prepared as described above, starting from 0.54 mmol of HL4. The product was obtained as an army green powder 0.2814 g (56%). Elemental analysis, exp (calc.): C 58.42 % (58.61%), H 3.08% (3.20%), N 8.49% (8.54%). ESI-MS, *m/z*, found (calc.): 719.2 (719.1) $[Cu(phen)_2(L4)]^+$ (Fig. S4). FT-IR (KBr), cm^{-1}: 1715 ($\upsilon(CO)_{ester}$), 1608 ($\upsilon(OCO)_{asym}$), 1396 ($\upsilon(OCO)_{sym}$).

$[Cu(phen)_2(L^5)](ClO_4)$ (D5) was prepared as described above, starting from 0.52 mmol of HL5**.** The product was obtained as a pale blue powder. 0.3517 g (90%). Elemental analysis, exp. (calc.): C 57.25 % (57.15%), H 3.13% (3.33%), N 7.29% (7.41%). ESI-MS, *m/z*, found (calc.): 656.1 (656.1) $[Cu(phen)_2(L5)]^+$ (Fig. S5). FT-IR (KBr), cm^{-1}: 1722 ($\upsilon(CO)_{ester}$), 1612 ($\upsilon(OCO)_{asym}$), 1373 ($\upsilon(OCO)_{sym}$).

$[Cu(phen)_2(L^6)](ClO_4)$ (D6) was prepared as described above, starting from 0.16 mmol of HL^6. The product was obtained as a pale blue powder. 0.1006 g (83%). Elemental analysis, exp. (calc.): C 56.97 % (57.15%), H 3.24% (3.33%), N 7.47% (7.41%). ESI-MS, *m/z*, found (calc.): 656.0 (656.1) $[Cu(phen)_2(L6)]^+$ (Figure S6). FT-IR (KBr), cm^{-1}: 1714 ($\boldsymbol{\upsilon(CO)_{ester}}$), 1608 ($\boldsymbol{\upsilon(OCO)_{asym}}$), 1401 ($\boldsymbol{\upsilon(OCO)_{sym}}$).

Cell culture conditions. SKOV-3 cells were cultured in high glucose (4.5 g/L) Dulbecco's Modified Eagle Medium (DMEM), enriched with 10% Foetal Calf Serum (FCS) and 1% of Penicillin/Streptomycin sulphate at 37 °C in humidified atmosphere containing 5% of CO_2. Stock solutions of the studied compounds were prepared in DMSO at 2.0 mM concentration.

Cell viability assay. Cells were cultured for 24 hrs on a 96-well plate at a density of 5000 cells per well in medium containing the studied compounds at the indicated concentrations. DMSO was used as a control. Then, the MTT reagent was added directly to the culture medium for 3 hrs. Then, medium including MTT reagent was aspirated, and the cells lysed by addition of 90% isopropanol, 0.04 M HCl and 10% Tween-20. Absorbance was measured at 570 nm by a Synergy HTX multi-mode reader (BioTek Instruments, VT, USA). All measurements were performed in technical hexaplicates and repeated in three independent experiments. Statistical significance between the treatments and the control was evaluated using Graph Pad Prism 8 using the Student's t-test.

SDS-PAGE and western blotting. SKOV-3 Cells were incubated with the studied compounds at 1.0 and 2.0 µM concentrations for 24 hrs using DMSO as control. Cells were washed twice with PBS and lysed with SDS lysis buffer (100mM TRIS-HCl pH 7.4, 1% SDS, 10% glycerol). Protein content in the cell extract was

quantified using the Bradford-based BioRad protein Assay Kit. Cell extracts were mixed with 2×Laemmli sample buffer (100 mM Tris pH 6.8, 4% SDS, 200 mM DTT, 20% glycerol, and 0.1% bromophenol blue) and boiled for 5 min. An equivalent of 10 µg proteins was resolved using 10% sodium dodecylsulfate polyacrylamide gel electrophoresis (SDS-PAGE). Resolved proteins were electroblotted onto a 0.45 mm polyvinylidene difluoride (PVDF) membrane (Millipore, Czech Republic) and incubated with the indicated primary antibodies diluted 1:1000 at 4 °C overnight (Actin cat. no: Ab1801, from Abcam, UK; CHOP #2895 and BiP #3177; from Cell Signalling, MA, USA). Blots were developed using horseradish peroxidase (HRP)-conjugated anti-rabbit HRP #7074 or anti-mouse HRP #7076 (both Cell Signaling, USA) secondary antibodies, diluted 1:7500, and ECL plus (GE Healthcare) according to manufacturer's protocol. Results were visualized using a ChemiDoc® Touch Imaging System (Bio-Rad).

Author Contributions

Conceptualization: S.M., M.G.C., P.V., T.P.; Methodology: S.M., M.G.C., P.V., L.M, M.B., J.H., E.C., T.P.; Investigation: S.M., M.G.C., L.M., T.V.; Formal analysis: S.M., M.G.C., L.M., T.V.; Validation: S.M., M.G.C., L.M., M.B., T.V.; Visualization: S.M.; Writing – original draft: S.M.; Writing – review and editing: S.M., T.P., L.M., M.B., P.V.; Resources: T.P., M.G.C., E.C., M.B., J.H., P.V.; Supervision: S.M., T.P., P.V.

Conflicts of interest

There are no conflicts to declare.

Acknowledgements

S.M. thanks MIUR for his PhD fellowship (XXXIV cycle). We acknowledge the CeSAR (Centro Servizi Ricerca d'Ateneo) core facility of the University of Cagliari and Dr Sandrina Lampis for assistance with the generation of NMR data. L.M. is supported by funds from the Faculty of Medicine MU to junior researcher (Lukáš Moráň, ROZV/28/LF/2020), and Brno PhD Talent scholarship holder, funded by the Brno City Municipality. L.M. and M.B. acknowledge support by MH CZ-DRO (Masaryk Memorial Cancer Institute, 00209805). Mass Spectrometry CF of FNUSA-ICRC is acknowledged for the support and assistance in this work.

References

1 B. Rosemberg, L. Vancamp, J. E. Trosko and V. H. Mansour, *Nature*, 1969, **222**, 385–386.

2 P. J. Loehrer, *Ann Intern Med*, 1984, **100**, 704.

3 N. Eckstein, *Journal of Experimental & Clinical Cancer Research*, 2011, **30**, 91.

4 S. Dhar, F. X. Gu, R. Langer, O. C. Farokhzad and S. J. Lippard, *Proceedings of the National Academy of Sciences*, 2008, **105**, 17356–17361.

5 J. Michels, I. Vitale, L. Galluzzi, J. Adam, K. A. Olaussen, O. Kepp, L. Senovilla, I. Talhaoui, J. Guegan, D. P. Enot, M. Talbot, A. Robin, P. Girard, C. Orear, D. Lissa, A. Q. Sukkurwala, P. Garcia, P. Behnam-Motlagh, K. Kohno, G. S. Wu, C. Brenner, P. Dessen, M. Saparbaev, J.-C. Soria, M. Castedo and G. Kroemer, *Cancer Res*, 2013, **73**, 2271–2280.

6 F. Trudu, F. Amato, P. Vaňhara, T. Pivetta, E. M. Peña-Méndez and J. Havel, *J Appl Biomed*, 2015, **13**, 79–103.

7 R. Gil-García, M. Ugalde, N. Busto, H. J. Lozano, J. M. Leal, B. Pérez, G. Madariaga, M. Insausti, L. Lezama, R. Sanz, L. M. Gómez-Sainz, B. García and J. García-Tojal, *Dalton Transactions*, 2016, **45**, 18704–18718.

8 S. Dilruba and G. V. Kalayda, *Cancer Chemother Pharmacol*, 2016, **77**, 1103–1124.

9 T. J. P. McGivern, S. Afsharpour and C. J. Marmion, *Inorganica Chim Acta*, 2018, **472**, 12–39.

10 C. Marzano, M. Pellei, F. Tisato and C. Santini, *Anticancer Agents Med Chem*, 2009, **9**, 185–211.

11 C. Santini, M. Pellei, V. Gandin, M. Porchia, F. Tisato and C. Marzano, *Chem Rev*, 2014, **114**, 815–862.

12 S. Masuri, P. Vaňhara, M. G. Cabiddu, L. Moráň, J. Havel, E. Cadoni and T. Pivetta, *Molecules*, 2022, **27**, 49.

13 T. Pivetta, F. Isaia, G. Verani, C. Cannas, L. Serra, C. Castellano, F. Demartin, F. Pilla, M. Manca and A. Pani, *J Inorg Biochem*, 2012, **114**, 28–37.

14 T. Pivetta, F. Trudu, E. Valletta, F. Isaia, C. Castellano, F. Demartin, R. Tuveri, S. Vascellari and A. Pani, *J Inorg Biochem*, 2014, **141**, 103–113.

15 L. Moráň, T. Pivetta, S. Masuri, K. Vašíčková, F. Walter, J. Prehn, M. Elkalaf, J. Trnka, J. Havel and P. Vaňhara, *Metallomics*, 2019, **11**, 1481–1489.

16 S. Masuri, E. Cadoni, M. G. Cabiddu, F. Isaia, M. G. Demuru, L. Moráň, D. Buček, P. Vaňhara, J. Havel and T. Pivetta, *Metallomics*, 2020, **12**, 891–901.

17 I. Kostova, S. Bhatia, P. Grigorov, S. Balkansky, V. S. Parmar, A. K. Prasad and L. Saso, *Curr Med Chem*, 2011, **18**, 3929–3951.

18 S. Emami and S. Dadashpour, *Eur J Med Chem*, 2015, **102**, 611–630.

19 Y. Bansal, P. Sethi and G. Bansal, *Medicinal Chemistry Research*, 2013, **22**, 3049–3060.

20 O. Kayser and H. Kolodziej, *Zeitschrift fur Naturforschung - Section C Journal of Biosciences*, 1999, **54**, 169–174.

21 M. E. Marshall, J. L. Mohler, K. Edmonds, B. Williams, K. Butler, M. Ryles, L. Weiss, D. Urban, A. Bueschen, M. Markiewicz and G. Cloud, *J Cancer Res Clin Oncol*, 1994, **120**, S39–S42.

22 B. Thati, A. Noble, B. S. Creaven, M. Walsh, K. Kavanagh and D. A. Egan, *Eur J Pharmacol*, 2007, **569**, 16–28.

23 G. Deacon and R. J. Phillips, *Coord Chem Rev*, 1980, **33**, 227–250.

24 K. Nakamoto, *Infrared and Raman Spectra of Inorganic and Coordination Compounds*, John Wiley & Sons, Inc., Hoboken, NJ, USA, 2008.

25 E. Cadoni, E. Valletta, G. Caddeo, F. Isaia, M. G. Cabiddu, S. Vascellari and T. Pivetta, *J Inorg Biochem*, 2017, **173**, 126–133.

26 F.-X. Dong, *Acta Crystallogr Sect E Struct Rep Online*, 2011, **67**, o1105–o1105.

27 M. Devereux, M. McCann, J. F. Cronin, G. Ferguson and V. McKee, *Polyhedron*, 1999, **18**, 2141–2148.

28 F. Clifford, E. Counihan, W. Fitzgerald, K. Seff, C. Simmons, S. Tyagi and B. Hathaway, *J Chem Soc Chem Commun*, 1982, 196.

29 M. Barceló-Oliver, Á. García-Raso, Á. Terrón, E. Molins, M. J. Prieto, V. Moreno, J. Martínez, V. Lladó, I. López, A. Gutiérrez and P. V. Escribá, *J Inorg Biochem*, 2007, **101**, 649–659.

30 K. N. Lazarou, S. P. Perlepes, V. Psycharis and C. P. Raptopoulou, *Polyhedron*, 2008, **27**, 2131–2142.

31 T. Pivetta, E. Valletta, G. Ferino, F. Isaia, A. Pani, S. Vascellari, C. Castellano, F. Demartin, M. G. Cabiddu and E. Cadoni, *J Inorg Biochem*, 2017, **177**, 101–109.

32 T. Pivetta, S. Masuri, M. G. Cabiddu, C. Caltagirone, A. Pintus, M. Massa, F. Isaia and E. Cadoni, *New Journal of Chemistry*, 2019, **43**, 12032–12041.

33 M. Sirajuddin, S. Ali and A. Badshah, *J Photochem Photobiol B*, 2013, **124**, 1–19.

34 S. U. Rehman, T. Sarwar, M. A. Husain, H. M. Ishqi and M. Tabish, *Arch Biochem Biophys*, 2015, **576**, 49–60.

35 A. P. King and J. J. Wilson, *Chem Soc Rev*, 2020, **49**, 8113–8136.

36 R. Sano and J. C. Reed, *Biochim Biophys Acta Mol Cell Res*, 2013, 1833, 3460–3470.

37 T. Okada, H. Yoshida, R. Akazawa, M. Negishi and K. Mori, *Biochemical Journal*, 2002, **366**, 585–594.

38 T. Pivetta, F. Trudu, E. Valletta, F. Isaia, C. Castellano, F. Demartin, R. Tuveri, S. Vascellari and A. Pani, *J Inorg Biochem*, 2014, **141**, 103–113.

39 J. P., *Ann. Chim. Appl.*, 1928, **9**, 113–203.

40 J. S. Renny, L. L. Tomasevich, E. H. Tallmadge and D. B. Collum, *Angewandte Chemie International Edition*, 2013, **52**, 11998–12013.

41 J. Marmur, *J Mol Biol*, 1961, **3**, 208-IN1.

42 N. Raman, K. Pothiraj and T. Baskaran, *J Mol Struct*, 2011, **1000**, 135–144.

43 P. Gans, A. Sabatini and A. Vacca, *Talanta*, 1996, 1739–1753.

44 F. Isaia, M. C. Aragoni, M. Arca, C. Caltagirone, C. Castellano, G. De Filippo, A. Garau, V. Lippolis and T. Pivetta, *Green Chemistry*, 2017, **19**, 4591–4599.

45 T. H. J. Niedermeyer and M. Strohalm, *PLoS One*, 2012, **7**, e44913.

46 M. Strohalm, D. Kavan, P. Nova and M. Volny, *Anal Chem*, 2010, **82**, 4648–4651.

47 F. Neese, *Wiley Interdiscip Rev Comput Mol Sci*, 2012, **2**, 73–78.

48 M. D. Hanwell, D. E. Curtis, D. C. Lonie, T. Vandermeersch, E. Zurek and G. R. Hutchison, *J Cheminform*, 2012, **4**, 17.

49 C. Adamo and V. Barone, *Journal of Chemical Physics*, 1999, **110**, 6158–6170.

50 F. Weigend and R. Ahlrichs, *Physical Chemistry Chemical Physics*, 2005, **7**, 3297.

51 T. Y. Nikolaienko, L. A. Bulavin and D. M. Hovorun, *Comput Theor Chem*, 2014, **1050**, 15–22.

52 Chemcraft - graphical software for visualization of quantum chemistry computations. https://www.chemcraftprog.com.

53 O. Trott and A. J. Olson, *J Comput Chem*, 2009, 455–461.

54 G. M. Morris, H. Ruth, W. Lindstrom, M. F. Sanner, R. K. Belew, D. S. Goodsell and A. J. Olson, *J Comput Chem*, 2009, **30**, 2785–2791.

55 E. F. Pettersen, T. D. Goddard, C. C. Huang, G. S. Couch, D. M. Greenblatt, E. C. Meng and T. E. Ferrin, *J Comput Chem*, 2004, **25**, 1605–1612.

56 S. Masuri, M. G. Cabiddu, E. Cadoni and T. Pivetta, *New Journal of Chemistry*, 2021, **45**, 10749–10760.

57 Z. Gao, D. J. Maloney, L. M. Dedkova and S. M. Hecht, *Bioorg Med Chem*, 2008, **16**, 4331–4340.

58 A. Peperidou, S. Bua, M. Bozdag, D. Hadjipavlou-Litina and C. Supuran, *Molecules*, 2018, **23**, 153.

59 M. Mujahid, N. Trendafilova, A. F. Arfa-Kia, G. Rosair, K. Kavanagh, M. Devereux, M. Walsh, S. McClean, B. S. Creaven and I. Georgieva, *J Inorg Biochem*, 2016, **163**, 53–67.

60 Z. Gao, D. J. Maloney, L. M. Dedkova and S. M. Hecht, *Bioorg Med Chem*, 2008, **16**, 4331–4340.

61 T. Pivetta, V. Lallai, E. Valletta, F. Trudu, F. Isaia, D. Perra, E. Pinna and A. Pani, *J Inorg Biochem*, 2015, **151**, 107–114.